Seismic refraction study, single well test and physical core analysis of anthropogenic degraded Peat at the Badas Peat Dome, Brunei Darussalam

Revised draft manuscript for publication in

Engineering Geology

Muhammad 'Asri Akmal Bin Haji Suhip[1], Stefan Herwig Gödeke[1], Alexander R. Cobb[2], Rahayu Sukmaria Sukri[1]

[1] Universiti Brunei Darussalam, Brunei Darussalam

[2]Singapore-MIT Alliance for Research and Technology, Singapore

16 April 2020

Abstract

The Badas peat dome located in the Belait district is one of the biggest peat domes in Brunei, where most of the oil and gas industries are located. Over the years, this area has seen a noticeable loss of peatland due to fires and infrastructure development. In this paper, the anthropogenic effects on the Badas peat dome were studied for three survey areas using seismic refraction surveys, core analysis and single well tests. Satellite images were used to confirm the extent of past peat fires in the area. Using these methods, this study has identified multiple peat, sand and clay layers demonstrating the stratigraphic heterogeneity that can be present in tropical peatlands. In particular, a sand horizon underlying the peat deposits was identified, which has the potential to be a significant hydrogeological flow unit. Groundwater level interpretations from 2D velocity data were correlated to groundwater levels from coring. In order to determine the degradation impact on peat through lowering of groundwater levels using these methods we produced a subsurface reconstruction at two locations with different levels of peat degradation. Single well tests conducted in this study showed that disturbed peat had lower hydraulic conductivities with an average of 1.73×10^{-5} m/s compared to undisturbed peat with an average of 6.66×10^{-5} m/s. A combination of these methods (seismic refraction, single well test and coring) are suitable for identifying different levels of peat degradation. In addition, these methods can be suitable for profiling in tropical peatlands, for identifying groundwater levels as wells as identifying significant hydrogeological flow units.

Keywords: *Seismic Refraction, Coring, Tropical Peatland, Single Well Test, Peat Degradation*

Introduction

Intact peatlands are recognised as large waterlogged areas containing peat deposits with a minimum peat thickness of 30 cm containing at least 30% organic matter (Joosten & Clark 2002). Tropical peatlands, which are dome shaped when intact, contain more than 80% organic materials (James, 1984; Parish et al., 2008; Adon et al., 2012). These tropical peatlands cover between 275,000 km^2 to 575,000 km^2 worldwide with the highest percentage of around 41% found in South East Asia (Page et al, 2007; Warren et al, 2017).

Peatlands in South East Asia in particular have been declining, due to anthropogenic influences. They have been exploited by multiple industries involving logging, agriculture, road infrastructure and oil and gas development (Hooijer et al., 2010; Page et al., 2016; Lilleskov et al., 2018). As these peatlands start to be disturbed, e.g. through canals and ditches, groundwater levels start to drop (Figure 1). This drop in groundwater levels leads to physical compaction and peat oxidation as well combustion to which peat is highly susceptible during dry seasons (Usup et al., 2004; Hooijer et al., 2010; Lilleskov et al., 2018). Peat degradation associated with subsidence and combustion is an increasingly important global issue as peat swamp forests are invaluable ecosystems hosting a large variety of plants and animals (Posa et al, 2011; Marshall et al. 2018). Additionally, the large volume of undecomposed organic matter in peat plays a crucial role in regulating climate, as peat stores large amounts of carbon estimated to be 500-700 giga tons of the earth's carbon storage (Page & Hooijer, 2016). The South East Asian region alone stores 65% of tropical peat carbon which is equivalent to 105 Gt C (Warren et al., 2017).

Recently, the impact of precipitation on the CO_2 emissions and storage capacity of tropical peatlands has been investigated (Cobb et al., 2017), indicating that these peat domes have grown over thousands of years (Dommain et al., 2015). Recent research has shown that natural

63 tropical peat has a high hydraulic conductivity and is therefore particularly vulnerable to any
64 form of drainage or climate change (Baird et al., 2017, Cobb and Harvey, 2019).

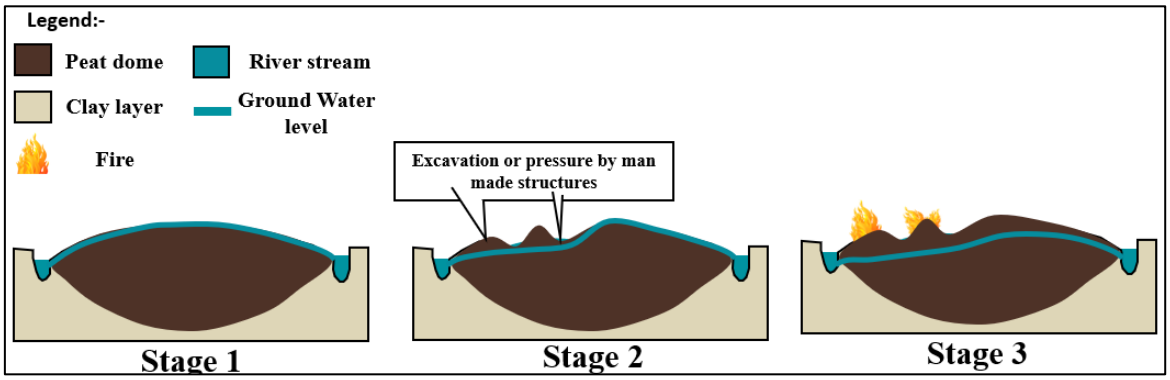

65

66 **Figure 1: Peat degradation stages (modified from Page et al., 2016)**

67 The resulting combustion of the dried peat destroys the habitat for plants and animals. It also
68 leads to the emission of stored carbon into the atmosphere as carbon dioxide, carbon monoxide,
69 methane and particulate matter (<10 µm) (Couwenberg et al, 2019; Hayasaka et al., 2016,
70 Kobayashi, 2016; Lilleskov et al., 2018)..

71 Brunei, a South East Asian country, is experiencing peat fires every year (Din et al., 2018)
72 often in the driest months of the year commonly February and March. Out of Brunei's total
73 land area of 5700 km^2, around 16% is covered with peatland found predominantly in the Belait
74 district (James, 1984; Page et al., 2006; Sandal, 1996). At the Badas peat dome, which has an
75 area of around 372 km^2, a research site to investigate peat deposits in detail has been
76 established. In particular urbanisation over the past 30 years is threatening further drainage of
77 peat and parts of the Badas peat dome have already been affected with roads cutting through
78 and pipelines running above the deposits.

79 With the possible increase of fire occurrences, studies on how anthropogenic disturbances in
80 tropical peatlands can affect the structure and water levels of peat are urgently needed, in order
81 to better understand peat degradation.

This study utilises seismic refraction surveys combined with coring and single well tests at multiple sites in Badas together with satellite imagery to better understand the anthropogenic impact on the peat deposits (Figure 2).

These methods were selected because they have been proven to be cost-effective with the seismic refraction method able to provide a subsurface picture even in challenging environments. These tools are also able to identify multiple lithological structures based on their geophysical and geotechnical properties (Bery & Saad 2012; Lukić et al., 2011). However very few studies exist which apply the seismic refraction methods for tropical peatlands in order to identify peat degradation as well as groundwater tables. Thus, the motivation for this study. Seismic refraction for peat is challenging due to high signal attenuation as well as challenging signal to noise ratios. Seismic velocities in peat are general lower compared to other sedimentary layers due to the peat's high void ratio and compressibility. Seismic refraction was previously successfully applied for investigation of a coastal aquifer in Brunei (Azhar et al, 2019), but has rarely been applied for peat deposits. Two previous studies applied the method, one for deposits with thinly interlayered peat (Grelle & Guadagno, 2009), the other one at a tropical peat swamp in Johor, Malaysia (Said et al, 2015).

Methodology

Study site

The study area (Figure 2) lies in the vicinity of the Seria By Pass road around 108 km from Brunei's capital city. A previous investigation at the Badas peat dome revealed peat thicknesses of up to 9.7 m (Stoneman 1997). The area can be recognized by two pipelines running across the peat dome. Noticeable anthropogenic changes such as land excavations and sand layers laid above the peat for road pathways have been identified, providing an ideal setting for studying anthropogenic peat degradation (Figure 2). Most of the area is covered by vegetation and unstable soft peaty soil. The mean waterlevel is around 0.4 m below the surface. The presence of pioneer ferns at the site is a clear indication that the site is recovering from fires. Three areas were surveyed and identified based on accessibility, flat and semi dry ground providing enough stability for equipment transport.

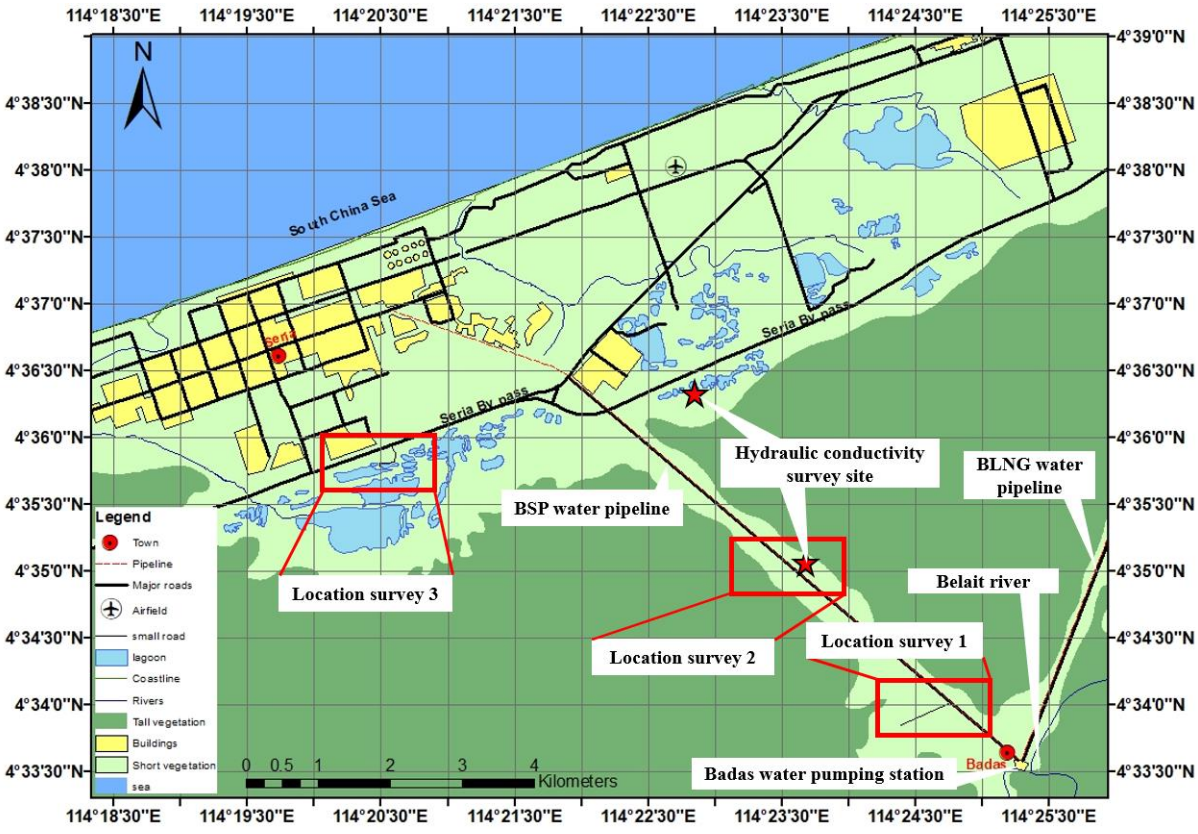

Figure 2: Location of study area with surveys locations

Seismic acquisition and configuration

For seismic data acquisition, a portable seismograph (Geometrics, SmartSeis) was used, with built-in computer screen, powered by a 12-volt battery. The SmartSeis was connected with 24 10 Hz vertical geophones via geophone connectors. Seismic energy was derived from a 6 kg sledgehammer which was struck onto a metal plate.

The main aim of the acquisition was to obtain a 2D velocity image of the subsurface. Each location has 13 shot points for improving the signal to noise ratio as well as to obtain better quality data (Figure 3). Coordinates and elevations of the planted geophones were recorded using a GPS (Garmin GPSmap 62, ??) .

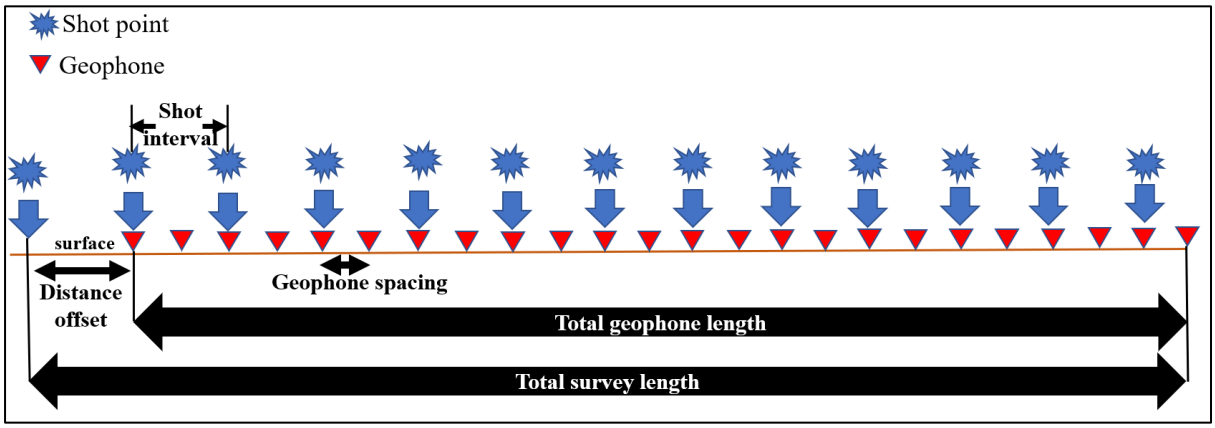

Figure 3: Seismic survey geometry

The total survey length varied for each location depending on geophone distance and offset configuration (Table 1). Variation of geophone distances and offset configurations were primarily for the purpose of collecting larger dimensions (depth and width) of 2D seismic data with good resolution. A previous study for a coastal aquifer in Brunei used geophone spacings of 5m (Azhar et al. 2019). For this study, geophone spacing was further reduced (2-3m) to achieve a better resolution. Referring to the table below (Table 1), locations 1 and 3 had identical geophone spreads of 72m with 3 shot stacks. These sites were judged as providing good conditions for seismic waves to travel through the subsurface without losing much energy. However, at location 2, the ground was much softer and semi wet. Therefore, geophone

spacing was reduced to 2 m and stacking increased to 5 in order to improve the signal to noise ratio and thus data quality.

Table 1: Seismic survey configuration and details

Parameter	Location 1	Location 2	Location 3
Data recorder	SmartSeis (Geometrics), 24 channels		
Seismic source	6 kg sledgehammer		
Geophone type	10Hz vertical geophone		
No. of geophones	24		
Sampling rate	0.25 ms		
Recording length	0.25s		
Geophone spacing	3m	2m	3m
Total survey length	72m	48m	72m
Total geophone length	69m	46m	69m
Offset distance	3m	2m	3m
Stacking	3	5	3
Shot intervals	6m	4m	6m
Shots location (m)	3, 9, 15, 21, 27, 33, 39, 45, 51, 57, 63, 69,72	2, 6, 10, 14, 18, 26, 30, 34, 38, 42, 46, 48	3, 9, 15, 21, 27, 33, 39, 45, 51, 57, 63, 69,72
Coring device	Spiral auger and Dutch auger	Russian peat corer	Spiral auger and Dutch auger

Seismic refraction theory

Initially, when the hammer connects to the strike plate, the seismic vibration will trigger acoustic waves travelling uniformly in all directions beneath the subsurface (Sharma, 1986). However, when these waves encounter another layer with a different medium than the previous, there will be a change in velocity (Sandal, 1996), as seismic wave propagation is dependent on Snell's law of refraction (Sharma, 1986).

The waves can be classified into primary waves (P-waves) and secondary waves (S-waves) (Fkirin et al, 2016). However, most refraction studies focus on P-waves as they travel much faster than secondary waves, reaching the geophones as the first arrivals (Kneiblher, 1985). The data collected is typically displayed in form of time-distance graphs (Figure 4).

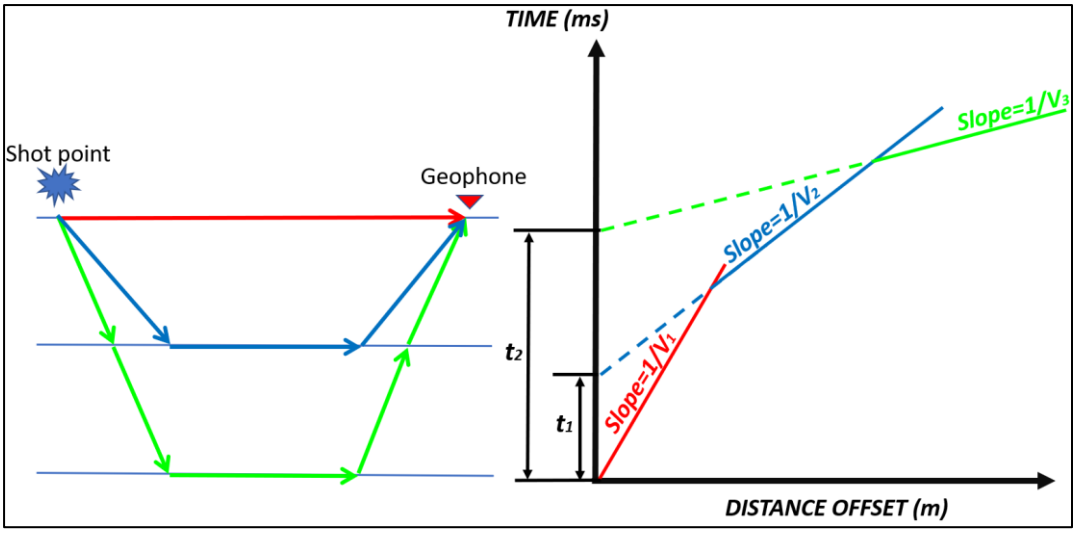

Figure 4: Pathway of seismic waves and time-distance graph representing the wave arrivals (modified after Azhar et al, 2019)

The velocity is estimated from the elapsed time until wave arrival as

$$v = \frac{\Delta t}{\Delta x} \quad (1)$$

where v= velocity of layer, Δx= distance offset (m) and Δt=elapsed time (milliseconds). The velocity can be used to estimate the thickness in each layer using the slope extension labeled t_1 and t_2 (Figure 4) also known as intercept time (t_{int}). The equation to estimate the layer 1 thickness is shown in equation 4, which is derived from equations 2 and 3.

$$t_{int_1} = \frac{x}{v_2} + \frac{2h_1\sqrt{v_2^2 - v_1^2}}{v_1 v_2} \quad (2)$$

$$h_1 = \frac{t_{int_1} v_1 v_2}{2\sqrt{v_2^2 - v_1^2}} \quad (3)$$

$$\mathbf{t_{int_1}} = \frac{\mathbf{2h_1\sqrt{v_2^2 - v_1^2}}}{\mathbf{v_1 v_2}} \quad (4)$$

After the first layer thickness calculation, thicknesses of deeper layers can be calculated with equation 5:

$$t_{int_2} = \frac{2h_1\sqrt{v_3^2 - v_1^2}}{v_1 v_3} + \frac{2h_2\sqrt{v_3^2 - v_2^2}}{v_2 v_3} \quad (5)$$

t_{int_x}= intercept time, v_1= velocity of layer 1, v_2 = velocity of layer 2, v_3=velocity of layer 3, h_1= layer thickness of layer 1, h_2 = layer thickness of layer 2

The calculated seismic velocities can be applied to interpret the sediment type and individual sediment layer thickness. The changing sediment velocities beneath the subsurface are related to corresponding changes in sediment densities (Keceli, 2012). A comparison of P-wave velocities for different sediments is shown in Table 2.

Table 2: P-wave velocities of earth materials (compiled from Fkirin et al., 2016; Bourbie et al., 1987; Said et al., 2015)

Types of soil, material	P-wave velocities (m/s)
Peat soil (dry to wet)	200-700
Dry sands	400-1200
Wet sands	1500-2000
Clay	1000-2500
Saturated clays	1100-2500
Sandstone	2000-6000
Saturated sandstones	2000-3000
Granite	5500-6000
Limestone	2500-6000
Air	330
Coal	2200-2700
Water	1450-1500
Ice	3400-3800
Oil	1200-1250
Steel	6100

The saturated layer has been interpreted based on the significant increase in p-wave velocities which occur when seismic waves cross from an unsaturated to a saturated unit.

Bulk density of the peat was calculated used the formula:

$$\rho = \frac{m}{v} \quad (6)$$

ρ = peat bulk density, m= mass of dried peat and v= volume of peat in the PVC

Seismic data processing

After data collection, recorded signals were analyzed by two of Seisimager/2D^{Tm} suite of software for seismic processing and interpretation. The first software, PickWin, is commonly used to determine first arrivals of seismic waves.

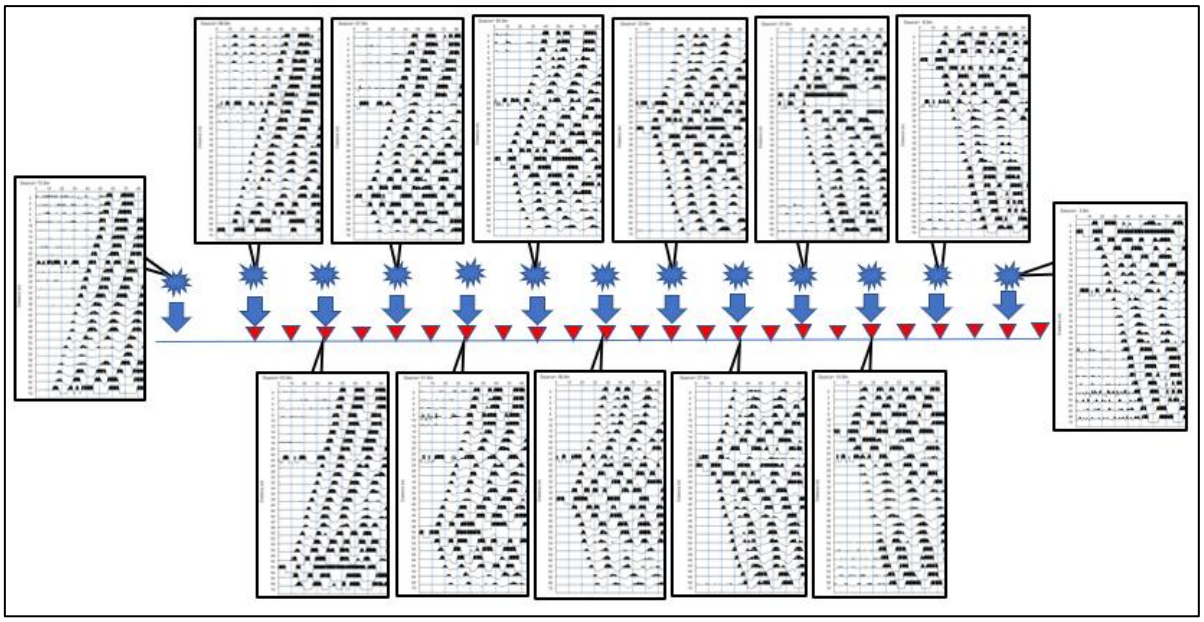

Figure 5: Example of raw data obtained from location 1

The data quality for location 1 was good with noticeable first arrivals and set as a quality standard for the other sites. Location 2 and 3 had a significant amount of seismic noise possibly resulting from natural man-made movements or from wind blowing into the vegetation converting it into ground vibrations. To decrease seismic noise low cut and high cut filters were applied to increase the signal to noise ratio. Low cut filters were used to filter low frequency waves below 38 Hz, while high frequencies above 512 Hz were filtered using high cut filter (Geometrics, 2009).

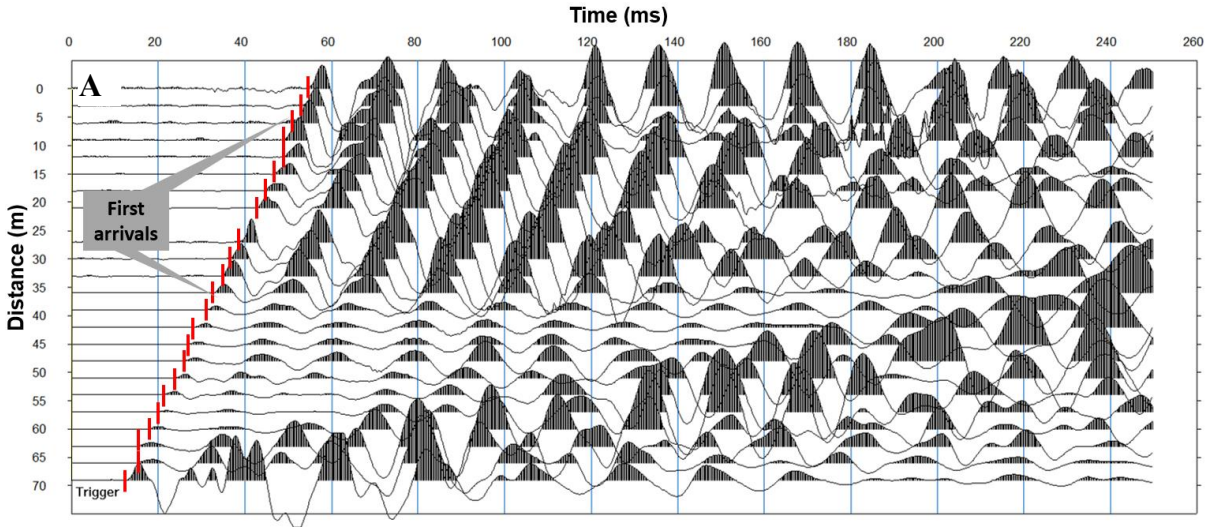

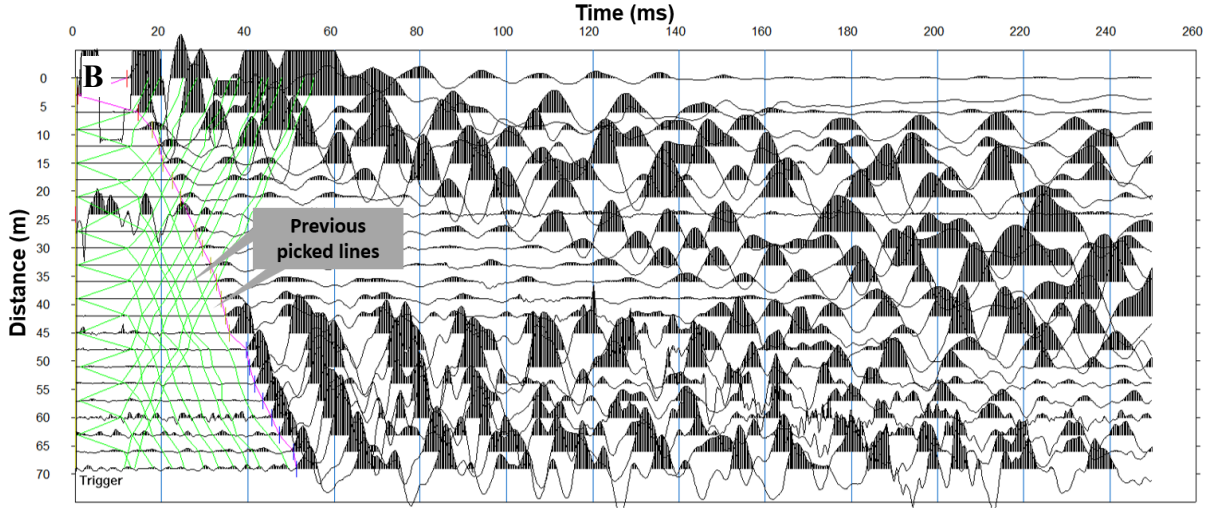

Figure 6: Example of first arrival picking of points (A, first shot) and (B, last shot) at location 1

Although the first arrivals selection could have been picked automatically, first arrivals were picked manually in order to avoid picking phantom arrivals (Redpath, 1973). An example of a time-distance graph is shown in Figure 7. A linear-least-squares approach was utilised to determine the best discrete layer solution for the data. If we define the "slowness" S as the inverse velocity we obtain:

$$S_1 = \frac{1}{V_1} \quad (7)$$

$$S_2 = \frac{1}{V_2} \quad (8)$$

211 And: $\sin(i_c) = \frac{S_2}{S_1}$ (9)

212 For a two-layer case and horizontal layering we can define the total travel time from source to
213 receiver with the above as:

214 $t = 2S_1 \cos(i_c) z + x S_2$ (10)

215 Defining: $c = 2S_1 \cos(i_c)$ (11)

216 We can write: $t = 2cz + xS_2$ (12)

217 With i_c as the critical angle and z and S_2 as unknown. The above assumes refractors parallel to
218 the surface. For curved surfaces we have an additional unknown z2, if we define z or z1 as the
219 depth between source and refractor and z2 as the depth between receiver and refractor. Thus,
220 we can write:

221 $t = cz1 + cz2 + xS2$ (13)

222 The above equation can then be solved in matrix form for all receivers and travel times.

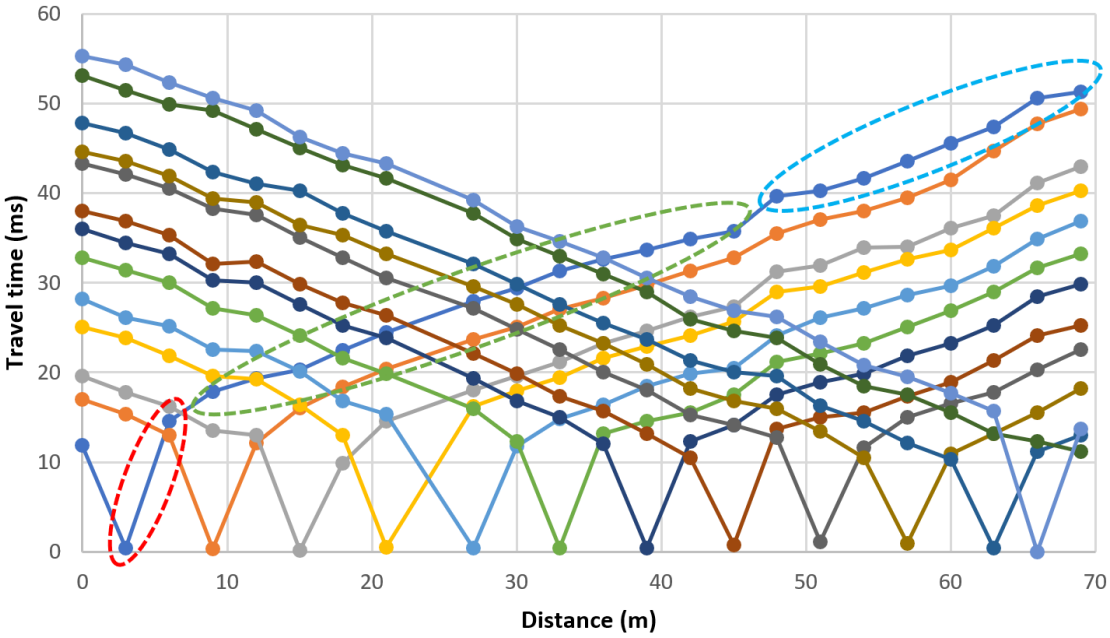

223

224 **Figure 7: Example of time-distance graph of location 1 with circled red (first layer) green (second**
225 **layer) and blue (third layer)**

Prior to the analysis of the seismic velocity profiles, the accuracy of the layer assignments was examined. In order for the velocity section to be valid for interpretation, the root mean square (RMS) error, between calculated and observed time vs. distance data, should not exceed the value of 1.5 ms (Geometrics 2009). None of the three velocity profiles exceeded the recommended RMS error threshold value (Table 3). Thus, the profiles were regarded as valid for data interpretation.

Table 3: Seismic processing RMS errors

Survey location	RMS error (ms)
1	0.39
2	1.18
3	1.05

Peat and sediment material examination

For an in-depth physical visualization and analysis of the subsurface materials, two hand augering and one coring devices were utilised. These equipment consist of a spiral auger, a Dutch auger and a Russian peat corer.

The coring and augering devices were useful in providing a ground truth correlation for the seismic data, which was processed beforehand. These hand boring equipment have their own purposes depending on the physical properties of the soil, with the Russian peat corer being the most suitable for soft waterlogged peat used primarily at location 2. A closing mechanism on the Russian peat corer retains the sample as the corer is pulled out of the peat. Meanwhile, both the Dutch and spiral augers were used for site 3. For this site, due to dry peat and dense sand it was very difficult to core to the same depth as at locations 1 and 2.

To collect the waterlogged, friable, peat cores, 5.08 cm diameter PVC pipes were cut vertically with a length interval of 50 cm having a volume of 572.56 cm^3 to match the dimension of the

247 Russian peat corer. A plastic wrapper was laid on the pipes to be wrapped around the core once
248 the core material is collected to prevent the loss of material and moisture during transportation.
249 The peat material was then placed carefully into the cut PVC pipe, hereafter referred to as core.

250 To determine the degree of peat degradation, the Von Post squeeze test (Von Post, 1922) can
251 provide a quick in situ examination based on its physical characteristics (Drzymulska, 2016).
252 The Von Post test can aid the sedimentary material analysis of a study (e.g. Adon et al, 2012;
253 Rahgozar et al., 2015).
254

255 **Single well tests (Slug and Bail)**

256 50 slug and 50 bail tests were conducted and hydraulic conductivities were analysed based on
257 the recorded pressure data. The in-situ slug and bail test were performed using a single well
258 piezometer made from a PVC pipe. The 2m long pipe dimensions are shown in figure 10, with
259 a 5.08 cm inner diameter and a screened section of 20 cm in length having 4 mm holes. The well
260 bore was hand drilled slightly smaller than the pipe with a Dutch auger (Supplementary Figure
261 1).
262 Although the hydraulic conductivity survey site (location 3) is at a distance from seismic survey
263 site 3, it has almost identical anthropogenic conditions (lagoons and road presence) so the
264 results will be taken as a representation for this seismic location.
265 For the tests, barometric pressure was recorded using a Solinst barologger Gold Model 3001
266 the absolute water pressure was recorded using a Solinst levelogger Junior Model 300. For
267 augered boreholes water levels were measured using a Solinst water level meter 101.

268 The well tests were conducted using a water filled T-pipe which was inserted and withdrawn
269 depending on the type of test. All the data for the slug and bail tests were recorded using one

second intervals (Supplementary Figure 2). The obtained data was then analysed using the Hvorslev (Hvorslev, 1951) and Bouwer and Rice (Bouwer and Rice, 1976) methods.

Results and interpretation

Location 1

From the velocity section in Figure 8 it can be seen that this location has a maximum depth of observation of around 14 m containing 3 layered structures. The first layer had a P-wave velocity of 391 m/s with an average thickness of 2m, located at an elevation of 3m above sea level (m.a.s.l.) to 1 m.a.s.l.. Based on the velocity, it was interpreted to be a peat layer (Table 2). The peat was correlated to the core section as seen in Figure 9, in which peat was found at depths of 0.5 m to 1.8 m. The sample had a low moisture content containing small amount of plant matter, as seen on the core section. The Von Post method determined the peat to have a H9 humification, indicating nearly completely decomposed peat (Supplementary Figure 3). Augering showed that the top layer is not solely peat as the top 0.5 m is sand placed for a road pathway. Thus, the seismic section contained a hidden layer which can occur if the above layer has a higher velocity than the layer below.

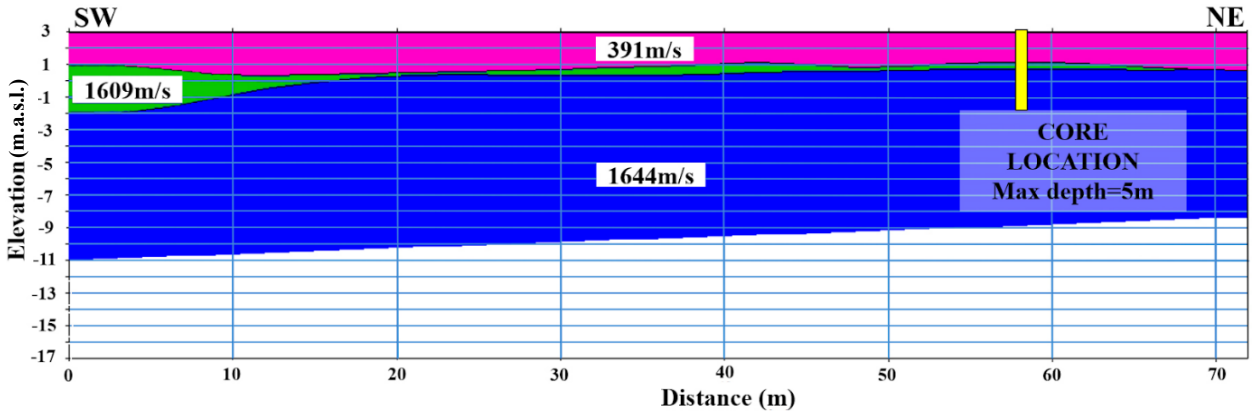

Figure 8: Seismic velocity profile of location 1 with location of 5 m core

The thickness of the peat in this location is much thinner in contrast to the peat layers of location 2 and 3. Due to the domal shape of the peatlands, the deposits are much thicker in

the center. This location which is in proximity of the Belait river is found near the edge of the peatland (Figure 2).

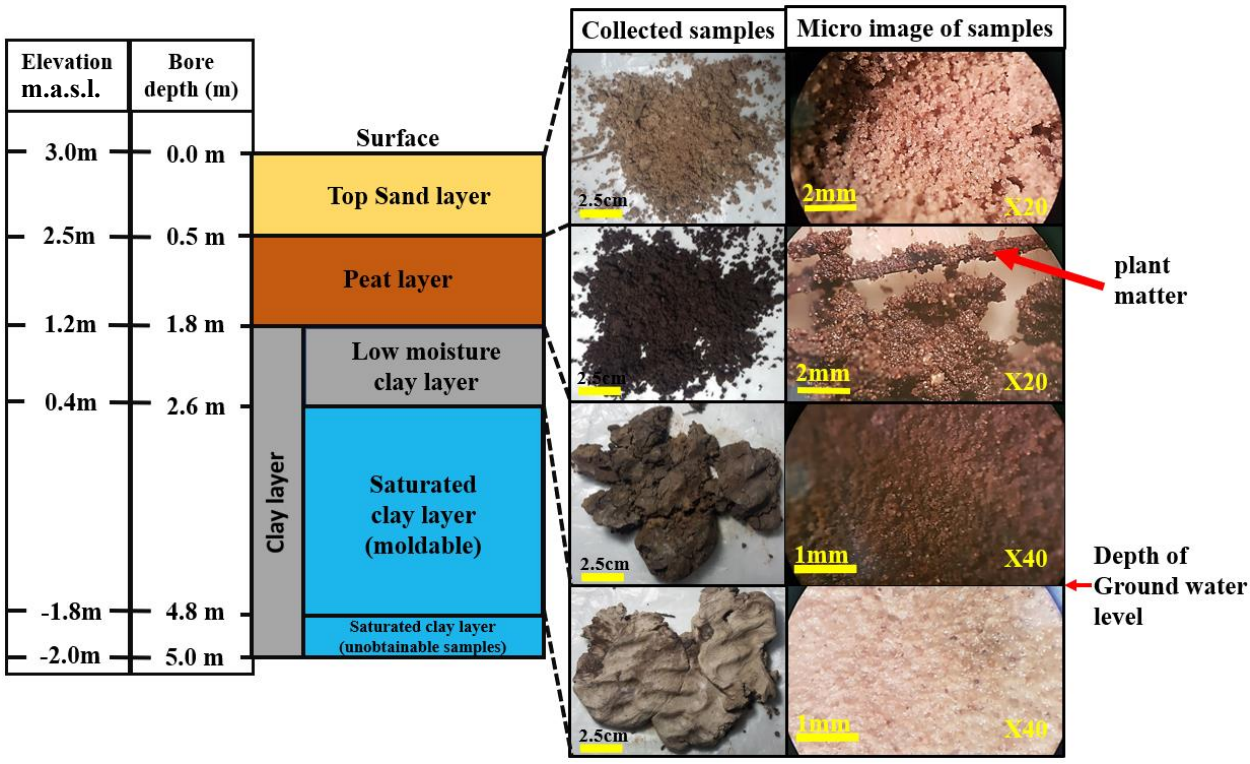

Figure 9: Subsurface material obtained from location 1

The second layer at location 1 was interpreted to be clay, having a velocity of 1609 m/s. This layer is thinning out towards the NE. The clay from the core obtained at a depth of 1.8m to 2.6m correlates to this layer. The collected clay sample had low moisture content with a hard non moldable physical property. The third layer showed a velocity of 1644 m/s which is also interpreted to be clay layer, becoming shallower towards the NE. It can be correlated to the clay obtained from the core at a depth of 2.6m. The collected clay however, had a different physical property than the clay from layer 2. The clay was easily moldable indicating saturated conditions. It was observed that the groundwater level was located at the top of this layer.

Location 2

The survey site at location 2 was the only area that showed low signs of peat degradation as its waterlogged condition was still intact. Three layers were detected in the seismic section as shown on Figure 10.

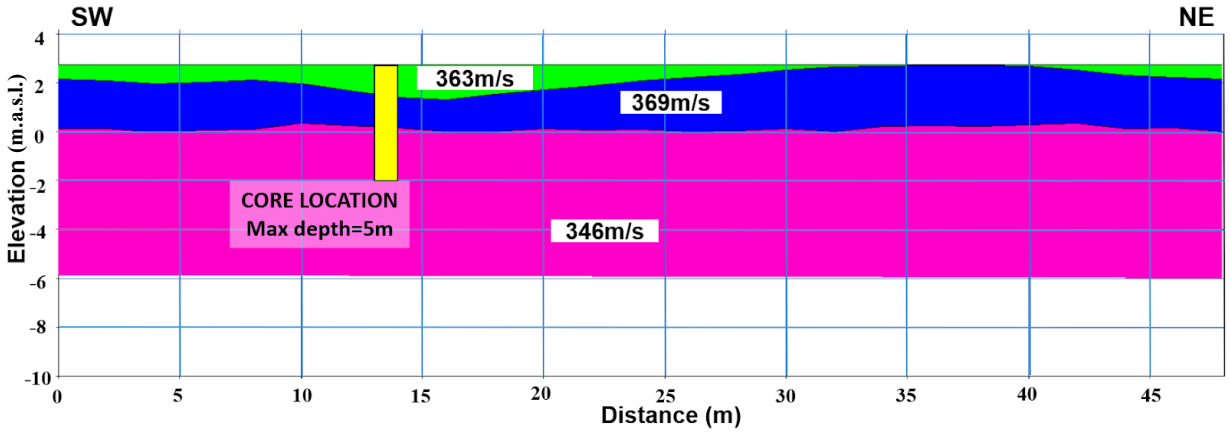

305

306 **Figure 2: Seismic velocity profile of location 2 with location of 5 m core**

307 The first layer had a velocity of 363 m/s and was found between the elevation of 3 m.a.s.l. to
308 2.5 m.a.s.l. The second layer showed a small increase in velocity with 369 m/s, located at a
309 depth of 2 m.a.s.l. to 0 m.a.s.l., however, some parts of this layer were exposed at the surface
310 at a survey distance between 32m to 41m. Lastly, the third layer showed a reduction in velocity
311 to 346m/s, with the layer found at an elevation of around 0 m.a.s.l..

312

313 All these layers were interpreted to be peat layers as they were within the range of peat P-wave
314 velocities (Table 2). The seismic velocity profile was correlated to a 5 m core that was air dried
315 for 1 week to determine the physical characteristics (Figures 11 and 12, Table 4). The first layer
316 of the seismic section with the velocity of 363 m/s is corelated to the core section between 0m
317 to 0.5m. The density of the peat core interval was also determined which showed a low density
318 of 0.057 g/cm^3 (Table 5). This core interval showed a significant shrinkage, in comparison to
319 the original size of the fresh core section (Figure 12). The drying efffect leads to the reduction
320 in pore space as water starts to escape (Oleszczuk, 2003). Therefore, a relatively high amount
321 of shrinkage compared to a lower amount of shrinkage of a particular peat sample indicates a
322 change in porosity. Thus, a high amount of shrinkage for a particular core section would
323 translate to an undecomposed or little decomposed peat with high porosity, as it can be seen in
324 this core section which contained small fragmented plant materials. The high amount of

shrinkage and the resulting lower seismic velocity between 2.5 to 5 m depth is in line with literature which points out the particular vulnerability of deeper peat layers to shrinkage (Schwärzel et al. 2002).

Table 4: Physical characteristics of core shown on Figure 11

Core depth	0.0m – 0.5m	0.5m – 2.5m	2.5m – 5.0m
Physical description	1. Amorphous friable peat 2. Contains small sized plant materials	1. Various medium sized intact roots, leaves and hard tissues 2. Groundwater level	1. Contains small to medium sized plant materials

Table 5: Dry bulk densities of core intervals of location 2

Core depth (m)	**Peat volume (cm3)**	**Peat mass (g)**	**Peat density (g/cm^3)**
0-0.5	506.71	29	0.057
0.5-1.0	506.71	44	0.087
1.0-1.5	506.71	34	0.067
1.5-2.0	506.71	48	0.095
2.0-2.5	506.71	42	0.083
2.5-3.0	506.71	23	0.045
3.0-3.5	506.71	33	0.065
3.5-4.0	506.71	36	0.071
4.0-4.5	506.71	27	0.053
4.5-5.0	506.71	36	0.071

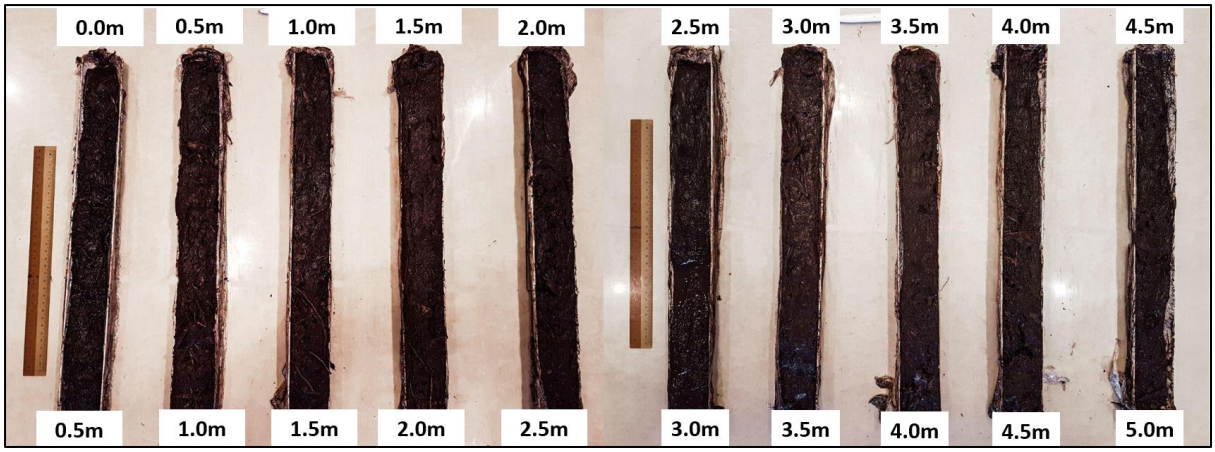

Figure 11: Core from location 2 before drying

Figure 12: Core from location 2 after drying

The increased velocity in layer 2 is interpreted to be due to the groundwater table located at the top of this layer as confirmed by coring. The watertable depth is in line with the mean watertable at the site. As the cores were dried, small reduction in size were observed only in between the depth intervals of 1.0m to 2.0m, showing that most of the spaces are occupied by a significant amount of large sized leaves, roots and other plant matter. The third layer at this location was correlated to the core interval of 2.5m to 5.0m, which showed a noticable reduction in size after drying. The drop in seismic velocity for this layer correlates with a drop in the average density to 0.054 g/cm^3 compared to 0.078 g/cm^3 of the above layer. The velocity

in the layer 3 decreased dramatically in contrast to layer 1. Since the geophones were planted on layer 1, the highest seismic energy was passing through this layer. When the seismic waves reached the fully saturated layer 2, the P-wave velocity increased further, but when the waves came into contact with layer 3, the waves started to dissipate due to the high amount of voids and less large plant matter in this layer in comparison to the second layer.

Location 3

The seismic section in Figure 13 shows that the first layer has an average velocity value of 366 m/s, identifying it to be a peat layer having an average thickness of 7.5m from the surface. Similar to location 1 this area also has a sand layer identifiable on the core section on figure 19 at a depth of 0.0m to 0.7m with peat present underneath it. The obtained peat material showed low moisture content with large amount of plant materials, such as microscopic fibrous plant matter and large woody tissues which may have come from tree trunks. These tree trunks caused difficulty in augering further than a depth of 1.5 m. The properties and the Von Post squeeze test done on the augered peat graded the layer to be H3 humification, indicating only a slight degree of decomposition.

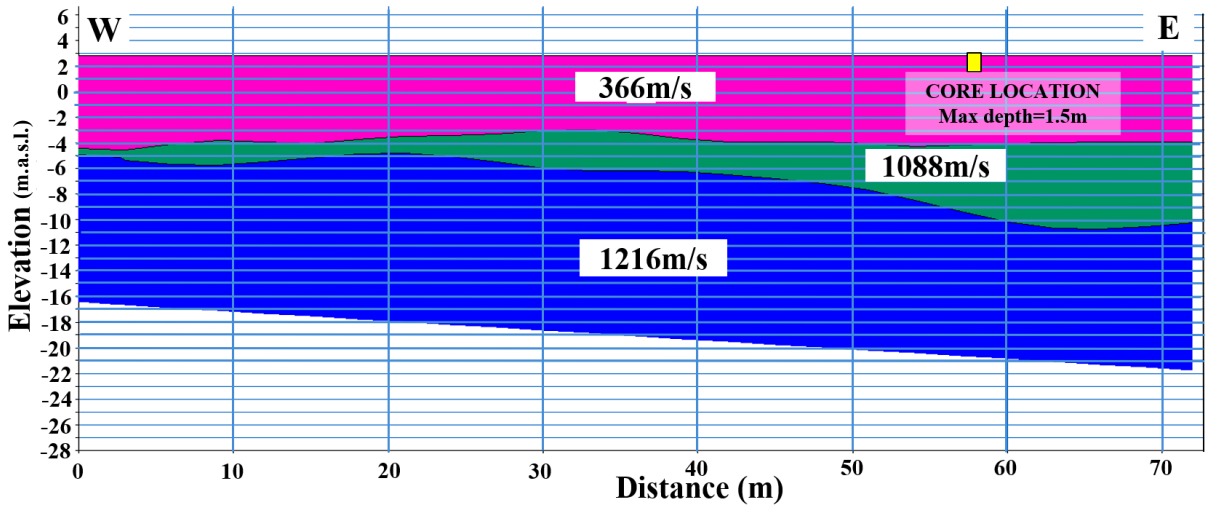

Figure 13: Seismic velocity profile of location 3 with location of 1.5m core

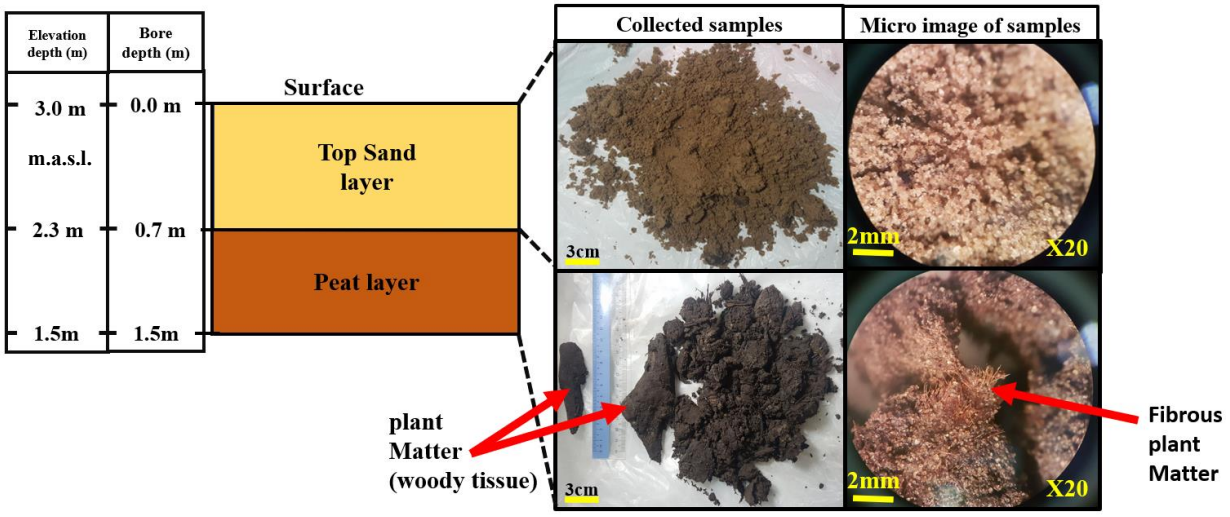

362 **Figure 14: Subsurface material obtained from location 3**

363 The second layer has a velocity value of 1088 m/s, made up of a thinner layer closer to the "F"
364 section of the velocity image, found at an elevation of -4 m.a.s.l. to -5 m.a.s.l, while thickening
365 towards the "E" section having a depth of -4 m.a.s.l. to -10 m.a.s.l.

366 The third layer with its top deepening towards the east has a P-wave velocity of 1216 m/s and
367 is identified as a silty clay layer based on its velocity which is lower but more similar to the
368 clay layer velocity at location 1 than to any of the peat layer velocities.

369 **Single well tests**

370 At location two, 42 well tests show a range from 10^{-6} m/s to 10^{-4} m/s with an average hydraulic
371 conductivity of 6.66 x 10^{-5} m/s. The remaining nine tests were performed at more degraded
372 peat near the Bandar-Seria Bypass road showed a ranged value of 10^{-6} m/s to 10^{-5} m/s with an
373 average conductivity of 1.73 x 10^{-5} m/s. All tests were performed at a depth of around 1 m
374 below the surface. Generally, these values are in the range of reported hydraulic conductivities
375 for tropical peat (e.g. Baird et al. 2017). The results show that hydraulic conductivities from
376 location 2 were higher than at location 3 where the peat is more degraded due to the influence
377 of the road and possible more pronounced subsidence. More single well tests need to be
378 performed in order to prove that the hydraulic conductivities between the different areas are
379 statistically different.

Discussion

Degradation of peatland is commonly associated with drainage causing loss of water from peat pores and shrinkage through drying. This results in an increase in bulk density commonly exacerbated by the resulting aerobic conditions causing peat degradation due to oxidation, as well as increased microbial decomposition, and compaction (Könönen et al., 2015). Investigations have shown that peat bulk density in tropical peatland increases due to drainage next to canals as well due to deforestation and fires (Sinclair et al. 2020). A drainage ditch exists next to the Badas pipeline which is around 1 to 1.5 m deep. Local attempts have been made to block this canal and backfill it. Increase in bulk density as well as compaction have an effect on the seismic velocity, which makes seismic refraction a tool to investigate peat degradation.

Location 1

From the results obtained at location 1 the peat layer showed degradation due to the falling of groundwater levels to a depth of around 2.6 m below the surface. This may have been caused by a large peat fire which occurred on 27th June 2014 (Figure 16). Smaller fires can be seen on the satellite image, dated 15th August 2013 and may have been initiated from the proximity of the road infrastructure and pipeline which caused drainage to the underlying layers mentioned in the introduction (Supplementary Figure 4). Furthermore, on 18th March 2016 a pathway was made with sand covering the degraded peat which causes an increased pressure on the peat, likely causing an additional lowering of the groundwater table of around 0.4 m, evident from the low moisture peat and clay obtained through augering.

Location 2

A location 2 satellite image dated from 14th July 2001 is shown on Figure 15. It becomes obvious that a fire occurred within the area increasing the ash content and possibly lowering the density of the first layer. The image also shows that the fire may also have originated near

the road and pipeline as discussed earlier. The results show that despite relatively undegraded peat present, previous burning events have impacted the site. The deeper peat layers may still be intact with low signs of degradation evident from low seismic velocities and fully saturated conditions. The variable pore structure seen during coring of these layers may have been related to the paleo-depositional environment.

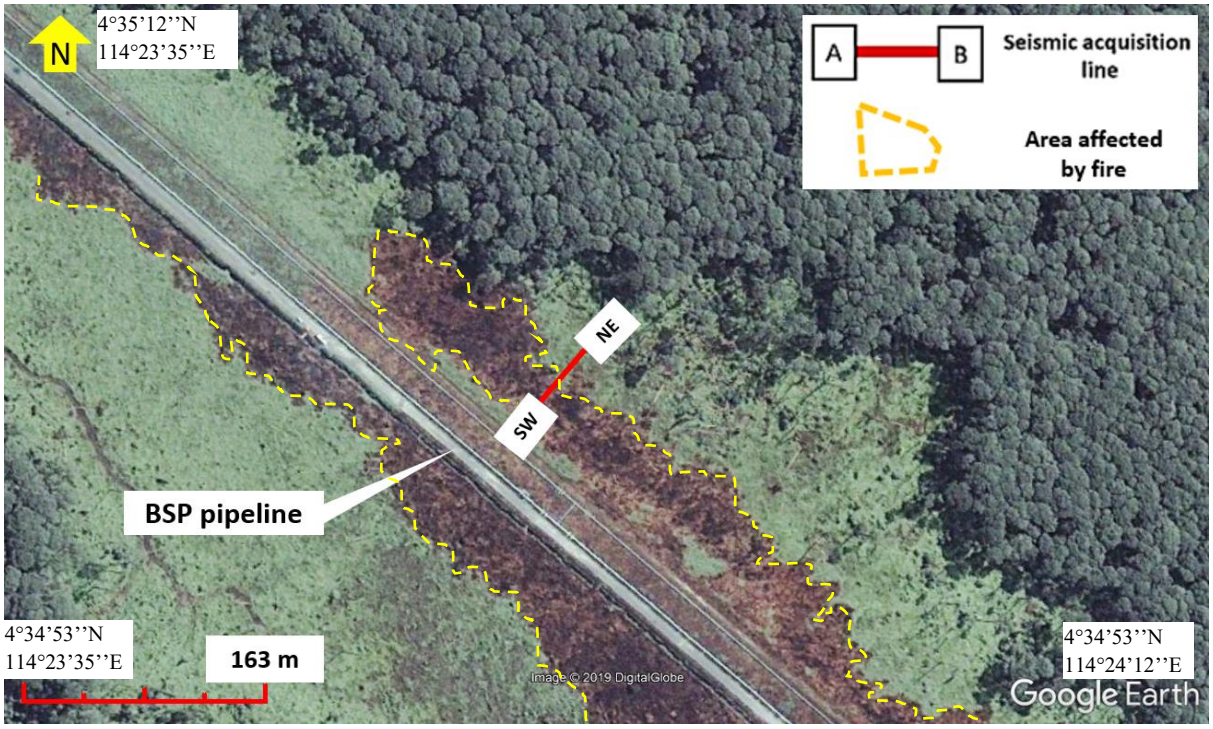

Figure 15: Satellite image (2001-07-14) modified from Google maps indicating peat fire

Location 3

Here, the top layer is clearly dry peat. The groundwater depth as well as deeper layers in this location have not been determined from coring due to the difficulty in coring beyond 1.5m from the surface. However, based on previous geotechnical drilling for the construction of the Seria Bypass Road in the direct proximity, the second and third layer are interpreted as sand and silty clay layers respectively (Techno Advance Laboratory 2009). The presence of a sand layer visualized through seismic refraction beneath the peat is a significant find, because it could represent an important hydrogeological flow unit. The third layer is interpreted as silty clay as most of the peat in the proximity of the Baram delta are predominantly underlain by

clayey sediments originating from rivers (Anderson,1964). When the Seria Bypass road was constructed in 2010, peat was excavated to a depth of around 4 m and the road was placed on the natural sand layer. The water can drain freely underneath the road through the sand layer. Further sand was excavated in the proximity for the road construction. These borrow pits from sand excavation are now visible as lagoons. Thus, the lagoons are not representative of the natural groundwater table but rather represent a perched groundwater table as the water is ponding directly on clayey substrate since peat and sand have been excavated prior at these locations. Therefore, based on our interpretation the groundwater is located at the top of the third layer around 7 to 8 m from the surface.

Thus, the deep groundwater table at this site is related to the degradation of peat associated with peat dugouts and drainage associated with the construction of the Bypass Road. From satellite images it becomes obvious that peat was excavated over a number of years. This excavation led to drainage, declining groundwater tables and peat fires (Figure 17).

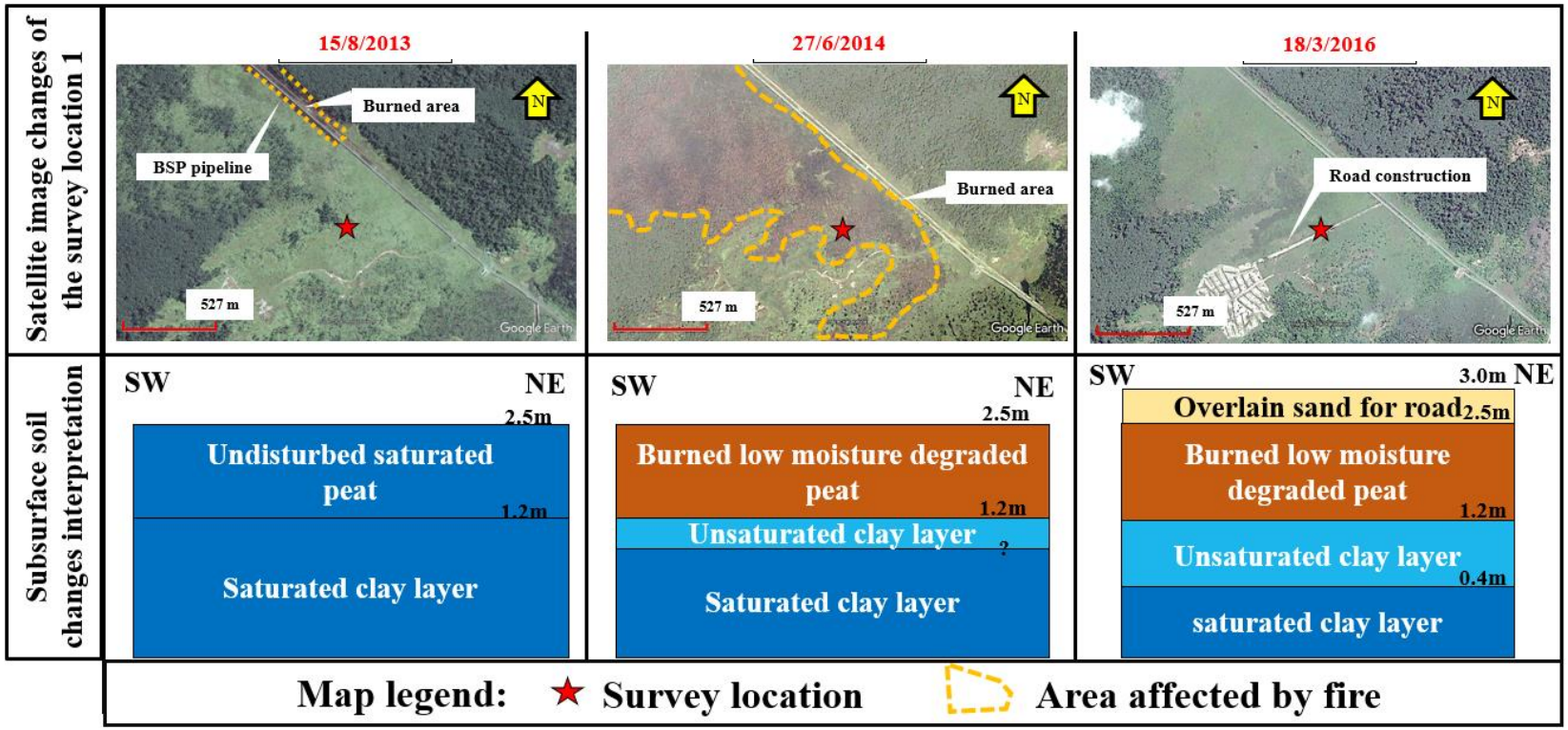

434

435 **Figure 16: Satellite image of land changes in location 1 modified from Google maps with subsurface illustration**

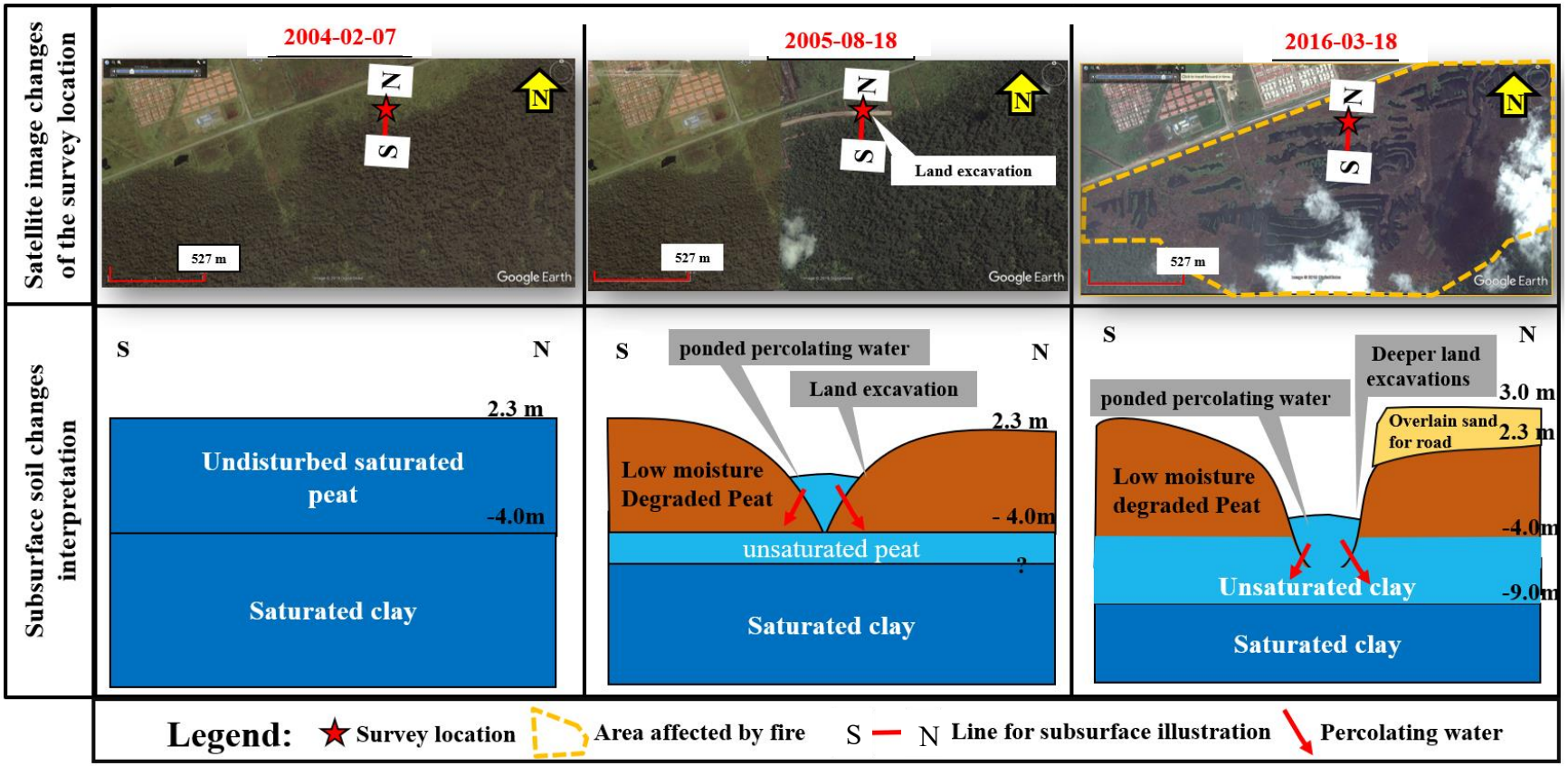

436

437 **Figure 17: Satellite image of land changes in location 3 modified from Google maps with subsurface illustration**

Conclusion

In this study seismic refraction, coring as well as single well testing was performed to characterize peatlands and identify different levels of degradation.

In particular the seismic refraction method can be applied for profiling in tropical peatlands and is able to identify different stratigraphies such as sand, clay and peat. In addition, groundwater levels can be identified.

The study showed that groundwater levels were significantly lower at sites where peat degradation was higher (site 1 and 3), compared to sites where peat degradation was considered low (site 2). The more degraded peat sites (1 and 3) also showed comparatively higher seismic velocities in particular for the first layer compared to the less degraded site. The single well tests performed at various locations aided in identifying comparatively undisturbed as well as disturbed anthropogenic influenced peat. In general, lower hydraulic conductivities were identified in more degraded peat, but more tests need to be done to confirm a statistical significance.

The integration of a number of methods with the usage of satellite imagery, allowed the identification and characterization of the impact of anthropogenic activities such as road construction and land excavation. The study identified a significant human impact on peat deposits at Badas, evident from the lowering of peat groundwater levels to a depth of up to 8 m below the surface to deeper clay layers. The identification of little-degraded and highly degraded peat in tropical peatlands will provide an insight to locating fire prone areas, which can assist in reducing more damage to peat deposits worldwide and aid in the focus of preserving peatlands for future studies.

Acknowledgements

This study was supported by the competitive research grant CRG # 18 from Universiti Brunei Darussalam and by the National Research Foundation Singapore through the Singapore-MIT Alliance for Research and Technology's Center for Environmental Sensing and Modeling interdisciplinary research program and Grant No. NRF2016-ITCOO1-021. The authors thank the Forestry Department, Ministry of Primary Resources and Tourism for granting a research permit for the Badas forest reserve. The authors thank Amal Nabilah Haji Matnoor, Hamisah Haji Piut, Abdul Muiz Hamdan, Zainulabidin Haji Mohammad and Zul Waqar Sarbini for fieldwork and data analysis. The authors thank Phua Eng Siong for IT support during this study.

Supplementary Material

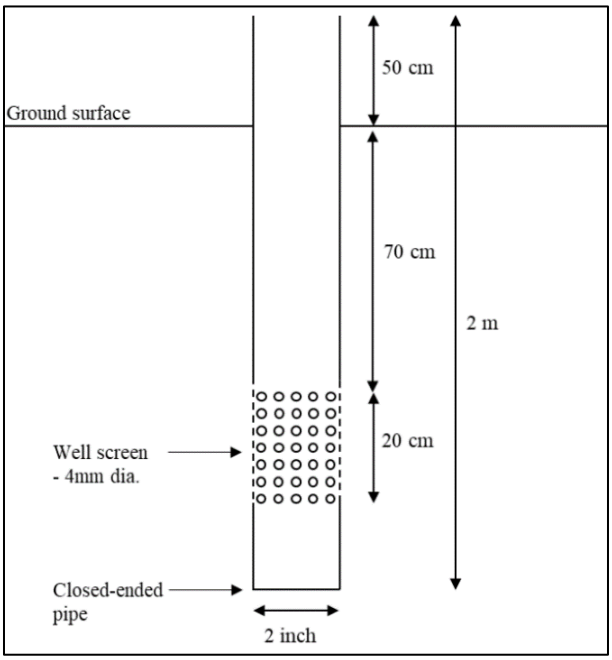

Supplementary Figure 1: Piezometer schematic for single well tests

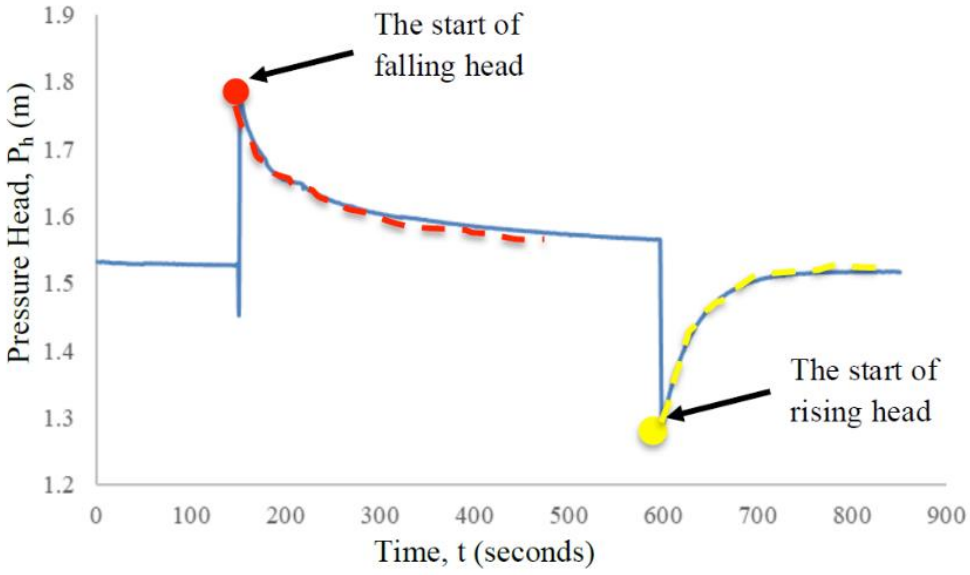

Supplementary Figure 2: Example of slug and bail test results

Supplementary Figure 3: Von Post test showing H9 peat humification

Supplementary Figure 4: Burnt vegetation within the proximity of the pipe structure (photo taken 24/2/2019)

References

Adon, R., Bakar, I., & Wijeyesekera, D. C. (2012). Overview of the Sustainable Uses of Peat Soil in Malaysia with Some Relevant Geotechnical Assessments, *International Journal of Integrated Engineering, 4*(3), 38–46.

Anderson J, A, R. (1964). The structure and development of the peat swamps of Sarawak and Brunei. *J Trop Geogr 18*:7–16.

Azhar, A.S., Latiff, A.H.A., Lim, L.H., Gödeke, S. (2019). Groundwater Investigation of a Coastal Aquifer in Brunei Darussalam using Seismic Refraction. Environ Earth Sci (2019) 78: 220. https://doi.org/10.1007/s12665-019-8203-6.

Baird, A.J., Low, R., Young, D., Swindles, G.T., Lopez, O.R., Page, S. (2017). High permeability explains the vulnerability of the carbon store in drained tropical peatlands. Geophys. Res. Lett. 44, 1333–1339. https://doi.org/10.1002/2016GL072245

Bery, A. A., & Saad, R. (2012). Correlation of seismic P-wave velocities with engineering parameters (N value and rock quality) for tropical environmental study. *International Journal of Geosciences, 3*(4), 749–757.

Bourbié, T., Coussy, O., & Zinszner, B. (1987). *Acoustics of porous media*. Houston, Texas: Gulf Publishing.

Bouwer H, Rice RC. (1976). A slug test for determining hydraulic conductivity of unconfined aquifers with completely or partially penetrating wells. Water Resources, 12(3), 423. doi:10.1029/WR012i003p00423

Cobb, A.R., Hoyt, A.M., Gandois, L., Eri, J., Dommain, R., Abu Salim, K., Kai, F.M., Haji Su'ut, N.S., Harvey, C.F. (2017). How temporal patterns in rainfall determine the geomorphology and carbon fluxes of tropical peatlands. Proc. Natl. Acad. Sci. 201701090. https://doi.org/10.1073/pnas.1701090114

530 Cobb, A.R., Harvey, C.F. (2019): Scalar Simulation and Parameterization of Water Table
531 Dynamics in Tropical Peatlands. Water Resources Research, Volume55, Issue11, pages
532 Pages 9351-9377
533
534 Couwenberg, J., Dommain, R,. and Joosten H. (2010). Greenhouse gas fluxes from tropical
535 peatlands in South-East Asia. Glob Change Biol 16: 1715-32
536
537 Din, H, H, M., Bakiri, N, B., Sukri, R, S., & Metali, M. (2018). Assessment of seedling
538 abundance, survival and growth of two dipterocarp species in peat swamp forests of
539 Brunei Darussalam, BIOTROPIA, 25(2), PP 148 – 154.
540
541 Dohong, A., Aziz, A, A, & Dargusch, P. (2017). A review of the drivers of tropical peatland
542 degradation in South-East Asia. Land Use Policy 69(October), 349–360.
543
544 Dommain, R., Couwenberg, J., & Joosten, H. (2010). Hydrological self-regulation of domed
545 peatlands in south-east Asia and consequences for conservation and restoration. Mires &
546 Peat, 6 (September 2014), 1–17.
547
548 Dommain R., Cobb A, R., Joosten, H., Glaser, P, H. , Chua, A, F, L., Gandois, L., Kai, F,M.,
549 Noren, A., Salim, K, A., Su'ut, N, S, H., Harvey, C,F. (2015). Forest dynamics and tip-up
550 poolsdrive pulses of high carbon accumulation rates in a tropical peat dome in Borneo
551 (Southeast Asia). J Geophys Res Biogeosci 120:617–640
552
553 Drzymulska, D. (2016). Peat decomposition – shaping factors, significance in environmental
554 studies and methods of determination; a literature review. Geologos, 22(1), pp 61–
555 69. doi:10.1515/logos-2016-0005
556
557 Fkirin, M, A., Badawy, S., & El deery, M, F. (2016). Seismic Refraction Method to Study
558 Subsoil Structure. J Geol Geophys 5: 259. doi: 10.4172/2381- 8719.1000259.
559
560 Geometrics Inc. (2009). SeisImager/2D Manual version 3.3 for PickWin and Plotrefa: October
561 541 2009, pp 1-25.

Grelle, G., Guadagno, F. M. (2009). Seismic refraction methodology for groundwater level determination: "Water seismic index." J Appl Geophys, 68(3), 301–320. https://doi.org/10.1016/j.jappgeo.2009.02.001

Hayasaka, H., Takahashi, H., Limin, S.H., Yulianti, N., Usup, A. (2016). Peat Fire Occurrence. Osaki, M., Tsuji, N. (eds.) Tropical Peatland Ecosystems, Springer. DOI 10.1007/978-4-431-55681-7_25

Hooijer, A., Page, S., Canadell, J. G., Silvius, M., Kwadijk, J., Wösten, H., & Jauhiainen, J. (2010). Current and future CO2 emissions from drained peatlands in Southeast Asia, Biogeosciences, 7, 1505-1514, https://doi.org/10.5194/bg-7-1505-2010.

Hvorslev, M.J. (1951). Time lag and soil permeability in ground-water observations, Bulletin 36, Waterways Experiment Station, Corporation of Engineers, United States Army, Vicksburg, Mississipi, 1-50.

James, D, M, D. (1984). The Geology and Hydrocarbon Resources of Negara Brunei Darussalam. 169 pp. Kota Batu, Brunei: Muzium Brunei; Seria, Brunei: Brunei Shell Petroleum.

Joosten, H., Clarke, D. (2002). Wise Use of Mires and Peatlands: Background and Principles Including a Framework for Decision-Making, 304 pages, ISBN 951-97744-8-3

Keceli, A (2012). Soil parameters which can be determined with seismic velocities, *Jeofizik, 16*, pp 17-29.

Kelly, T.J., Lawson, I.T., Roucoux, K.H., Baker, T.R., Jones, T.D., Sanderson, N.K., (2017). The vegetation history of an Amazonian domed peatland. Palaeogeogr. Palaeoclimatol. Palaeoecol. 468, 129–141. https://doi.org/10.1016/j.palaeo.2016.11.039

593 Kneiblher, C. R.(1985). *Seismic refraction surveys of alluvium-filled washes, Yucca Mountain,*
594 *Nevada* (Unpublished master's thesis), University of Nevada. Reno , USA.
595
596 Kobayashi, S. (2016). Peatland and Peatland Forest in Brunei Darussalam. In: Osaki M., Tsuji N.
597 (eds) *Tropical Peatland Ecosystems*. Springer, Tokyo.
598
599 Könönen, M., Jauhiainen, J., Laiho, R., Kusin, K., & Vasander, H. (2015). Physical and chemical
600 properties of tropical peat under stabilized land uses. Mires and Peat, 16(8), 1–13.
601
602 Lilleskov E, McCullough K, Hergoualc'h K, del Castillo Torres D, Chimner R, Murdiyarso
603 D, Kolka R, Bourgeau-Chavez L, Hribljan J, del Aguila Pasquel J, Wayson C (2018)
604 Is Indonesian peatland loss a cautionary tale for Peru? A two-country comparison of
605 the magnitude and causes of tropical peatland degradation. Mitig Adapt Strateg Glob
606 Chang. DOI: 10.1007/s11027-018-9790-3
607
608 Lukić, I., Barać, D., & Zovko, D. (2011). Seismic Refraction Method, International Balkans
609 Conference on Challenges of Civil Engineering.
610
611 Marshall, C., Large, D.J., Athab, A., Evers, S.L., Sowter, A., Marsh, S., Sjögersten, S., (2018).
612 Monitoring tropical peat related settlement using ISBAS InSAR, Kuala Lumpur
613 International Airport (KLIA). Eng. Geol. 244, 57–65.
614 https://doi.org/10.1016/j.enggeo.2018.07.015
615
616 Miettinen, J, Shi, C, and Liew, S, C. (2012). Two decades of destruction in Southeast Asia's peat
617 swamp forests, *Frontiers in Ecology and the Environment, 10*(3), pp. 124-128.
618
619 Oleszczuk, R., Bohne, K., Szatylowicz, J., Brandyk, T., & Gnatowski T (2003). Influence of load
620 on shrinkage behavior of peat soils. *J Plant Nutr Soil Sci 166*(2):220–224.
621
622 Page, S, E., & Hooijer A. (2016). In the line of fire: the peatlands of Southeast Asia. Phil. Trans.
623 R. Soc. B 371: 20150176, http://dx.doi.org/10.1098/rstb.2015.0176.

Page, S. E., Banks, C. J., Rieley, J. O., (2007). Tropical peatlands: distribution, extent and carbon storage-uncertainties and knowledge gaps. *Peatlands International, 2*(2), 26-27.

Page, S. E., Rieley, J. O., & Banks, C. J. (2011). Global and regional importance of the tropical peatland carbon pool. Global Change Biology, 17(2), 798 –818. doi:10.1111/j.1365-2486.2010.02279.x

Page, S, E., Rieley, J. O. & Wust, R. (2006). Lowland tropical peatlands of Southeast Asia.In: Martini, I.P., Martinez,C.A.& Chesworth,W.(eds.) Peatlands: Evolution and Records of Environmental and Climate Change, Elsevier BV, Amsterdam, The Netherlands, 145–172.

Parish, F., Sirin, A., Charman, D., Joosten, H., Minayeva, T., Silvius, M. & Stringer, L. (2008). Assessment on Peatlands, Biodiversity and Climate Change: Main Report Global Environment Centre, Kuala Lumpur and Wetlands International, Wageningen.

Redpath, B. B. (1973). Seismic refraction exploration for engineering site investigations. US Army Corps of Engineers, Technical Report E-73-4 10.2172/4409605

Rahgozar, M.A. & Saberian, M. (2015). Physical and chemical properties of two Iranian peat types. *Mires and Peat, 16* (07), 1–17.

Said M.J.M., Zainorabidin A., & Madun A. (2015). Soil Velocity Profile on Soft Soil Using Seismic Refraction, Applied Mechanics and Materials, Vols. 773-774, pp. 1549-1554,

Said M.J.M., Zainorabidin A., & Madun A. (2015). *Data Acquisition Challenges on Peat Soil Using Seismic Refraction.* In: Hassan R., Yusoff M., Alisibramulisi A., Mohd Amin N., Ismail Z. (eds) InCIEC 2014. Springer, Singapore.

655 Sandal, S, T. (1996). The Geology and Hydrocarbon Resources of Negara Brunei Darussalam.
656 (2nd ed.) Bandar Seri Begawan, Brunei Darussalam: Syabas.
657
658 Schwärzel, K., Renger, M.., Sauerbrey, R., Wessolek, G. (2002): Soil physical characteristics of
659 peat soils. J Plant Nutr. Soil Sci. 165, 479-486.
660
661 Sharma, P.,V. (1986). *Geophysical Methods in Geology*. 2nd Edition, Elsevier, Amsterdam.
662
663 Sinclair, A. L., Graham, L. L. B., Putra, E. I., Saharjo, B. H., Applegate, G., Grover, S. P., &
664 Cochrane, M. A. (2020). Effects of distance from canal and degradation history on peat bulk
665 density in a degraded tropical peatland. Science of the Total Environment, 699, 134199.
666 https://doi.org/10.1016/j.scitotenv.2019.134199
667
668 Stoneman, R. (1997): Ecological Studies in the Badas Peat Swamps, Brunei Darussalam. In:
669 Tropical Peatlands. Rieley, J. O. & Page, S. E. (Eds.), 1997, Samara Publishing Limited,
670 Cardigan, ISBN 1873692102
671
672 Surridge, B.W.J., Baird, A.J., Heathwaite, A.L., (2005). Evaluating the quality of hydraulic
673 conductivity estimates from piezometer slug tests in peat. Hydrol. Process. 19, 1227–1244.
674 https://doi.org/10.1002/hyp.5653
675
676 Techno Advanced Laboratory (2009): Unconsolidated Undrained (UU) Triaxial Test.
677 Unpublished Consulting Report, December 2009.
678
679 Usup A, Hashimoto Y, Takahashi H, Hayasaka H. (2004). Combustion and thermal
680 characteristics of peat fire in tropical peatland in Central Kalimantan, Indonesia.
681 Tropics V (1). 1-19. https://doi:10.3759/tropics.14.1
682
683 Von Post, L. (1922). Sveriges geologiska undersöknings torvinvenstering och några av dess
684 hittills vaanna resultant. Svenska Mosskulturfören. Tidskr. 36:1–27
685